Proceedings of International Conference on Heat Exchanger Fouling and Cleaning - 2013 (Peer-reviewed)
June 09 - 14, 2013, Budapest, Hungary
Editors: M.R. Malayeri, H. Müller-Steinhagen and A.P. Watkinson
Published online
www.heatexchanger-fouling.com

ORGANO SILICON AND TITANIUM OXIDE COATINGS FOR MITIGATION OF $CaCO_3$ DEPOSITIONS

E. Puhakka[1], E. Lecoq[2]

[1] VTT Technical Research Centre of Finland, P.O. Box 1000, FI-02044 VTT, Finland and E-mail: eini.puhakka@vtt.fi
[2] Department Science and Analyse of Materials, Centre de Recherche Public – Gabriel Lippmann, 41 rue du Brill, L-4422 BELVAUX, Luxembourg and Email: lecoq@lippmann.lu

ABSTRACT

Fouling reduces the thermal efficiency of heat transfer units, and it causes economic losses and has a marked effect on CO_2 releases and thus on climate change. In order to improve the energy efficiency, deposition formation (precipitation and crystallization) onto the heat transfer surfaces is going to be mitigated. A way to achieve this goal is the development of new surface materials with controlled chemical composition and morphology. In this study, formation mechanism of $CaCO_3$ depositions was investigated on modified (-CH_3 and –COOH) organo silicon (SiOC), and anatase and rutile TiO_2 surfaces. The results were compared to those of stainless steel surfaces. Based on the molecular modelling results, anatase and -COOH functionalized SiOC coatings are promising materials for mitigation of fouling caused by $CaCO_3$.

INTRODUCTION

Fouling reduces the thermal efficiency of heat transfer units and is still one of the major problems in most industrial processes. It causes economic losses and has a marked effect on carbon dioxide (CO_2) releases and thus on climate change. It has been estimated that fouling costs are about 0.2% of the countries' Gross National Product (Müller-Steinhagen, 2002).

In industrial processes, depositions of inversely soluble cationic salts, like calcium carbonate ($CaCO_3$), are rather typical depositions, which form unwanted depositions. Since $CaCO_3$ is inversely soluble in water, the water-soluble calcium loses its ability to remain in solution and precipitates as a hard solid on heated surfaces. This inverse solubility behaviour allows the salt to form an insulating deposit on the heat transfer surfaces. The deposit will then obstruct heat transfer, which leads to energy wastage and inhibition of fluid flow. Though, depositions are typically cleanable with pressure cleaning and acids, still costs of energy losses, operation and maintenance are significant. Because prevention of calcium depositions is difficult by controlling process conditions, new novel surface material are on development in order to mitigate fouling e.g. in dewatering and evaporation processes.

A prerequisite for a development of materials is that the adhesion mechanisms of depositions onto surfaces are known. Fouling mechanisms can be classified into six groups: crystallization, particle attachment, chemical fouling, corrosion, biological fouling and solidification (Bott, 1995; Mwaba et al., 2006). The fouling rate, the chemical composition and the physical properties of deposited material on the surfaces depend on process conditions (e.g. pH, temperature, concentrations of soluble species of particles, fluid flow) and construction materials of heat transfer surfaces (Kostoglou and Karabelas, 1998). In the case of $CaCO_3$ depositions, the role of crystallization fouling is the most probable mechanism in the initiation of the fouling.

It is demanding to gather information about interaction mechanisms (chemical or physical) between heat transfer surfaces and depositions with experimental methods. Therefore, we have utilized laboratory scale fouling experiments and molecular modelling in order to obtain explanations for the attachment of depositions at the molecular level (Puhakka et al., 2011; Puhakka et al., 2012; Pääkkönen et al., 2010).

Now, deposition formation was investigated on titanium oxide (TiO_2) and modified organo silicon (SiOC) surfaces. Coatings were synthesized using different deposition systems. Organo silicon coatings were prepared through atmospheric pressure - plasma enhanced chemical vapour deposition (AP-PECVD) while titanium oxide thin films were deposited by physical vapour deposition (PVD). The effect of the chemical composition of stainless steel surface on the deposition formation was also taken into account. The aim of the study was to clarify, if it is possible to use TiO_2 and modified SiOC coatings instead of pure stainless steel surface in order to avoid $CaCO_3$ depositions. The investigated coatings were selected based on industrial interest, when fouling caused by inversely soluble salts is attempted to mitigate on heat transfer surfaces.

METHODS

Molecular Modelling

Density functional methods were used to investigate surface oxide layer structures of stainless steel, titanium and silicon oxide coatings, and $CaCO_3$ deposition formation on these surfaces. Because real surfaces are subject to the effect of ambient process conditions, the role of process fluid (water) for surface structures was taken into account.

Therefore, the adsorption mechanism of water onto the surfaces was investigated, and thereafter the model surfaces for deposition formation studies were generated. All the calculations were performed with the CASTEP (Cambridge serial total energy package) code implemented into Materials Studio versions 5.0 (Accelrys, 2009) and 6.0 (Accelrys, 2011). In the calculations, the total electronic energy and overall electronic density distribution were solved in order to define the energetically stable structures for surfaces and adsorbates on the surfaces (Leach, 2001).

During the geometry optimization of the structures of stainless steel and coatings, and adsorption studies of water and calcium (Ca^{2+}) and carbonate (CO_3^{2-}) ions onto the surfaces, the exchange-correlation was described with generalized gradient approximation GGA-PBE. As a compromise between the accuracy and computational time of calculations, the ultrasoft pseudopotentials were used. In the potential of chromium, iron and titanium, the semicore states were treated as a part of the core. The used potentials were C_00PBE.usp for carbon, Ca_00PBE.usp for calcium, Cr_00PBE.uspcc for chromium, Fe_00PBE.uspcc for iron, H_00PBE.usp for hydrogen, O_soft00.usp for oxygen, Si_soft00.usp for silicon, and Ti_00.uspcc for titanium. The kinetic cut-off energy for a plane wave expansion of the wave function was 280 eV.

Energy values for the formation of $CaCO_3$ depositions were calculated from the single-point energies of the ions and the surface structures with and without the adsorbed ions. The calculations were performed using the GGA-RPBE exchange-correlation, and the kinetic cut-off energy was 330 eV.

Coating Techniques

Thin films were deposited on 316L stainless steel samples (50 mm x 50 mm x 2 mm) provided by Outokumpu for fouling tests. For characterization needs, thin films were also deposited on silicon substrates (100) and aluminium foils. However, growing of coatings can differ depending on the substrates. Prior to deposition, all the substrates were cleaned with hexane (10 min) and ethanol (10 min) in an ultrasonic bath.

Titanium oxide thin films. Inorganic TiO_2 thin films were deposited by direct current magnetron sputtering (dcMS). The deposition chamber (Fig. 1) contains four magnetrons and targets which are tilted by 30° to the normal. The substrate is placed on the rotating sample holder (8 rpm), in the middle of the chamber, at 90 mm from the targets. After sample introduction the vacuum chamber is pumped out by a turbomolecular pump down to a pressure of 5 x 10^{-7} mbar. Argon and oxygen are introduced in the chamber and the working pressure is adjusted by mean of a throttle valve to 6 x 10^{-3} mbar. Depositions were carried out from a titanium target (99.99% purity, 2 inches diameter, provided by neyco company) in reactive mode (30 sccm Ar + 8 sccm O_2) at a fixed power value of 450 W during 1h. After the deposition step, one of the prepared TiO_2 samples was annealed at 300 °C during 3 hours in order to get different morphology.

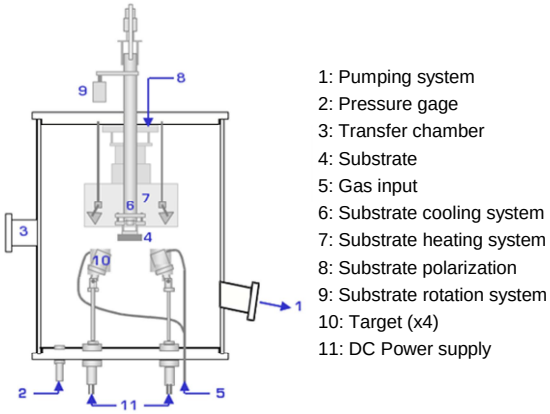

Fig. 1. Schematic of dcMS chamber.

Organo silicon thin films. Three different organo silicon coatings were prepared via AP-PECVD using two distinct reactors: a remote dielectric barrier discharge (DBD) reactor and a direct plane-to-plane DBD reactor (Fig. 2).

The remote-DBD reactor is manufactured by the company AcXys Technologies (France). It is electrically supplied by a 130 kHz sinusoidal high-voltage (HV) generator and presents a cylindrical coaxial geometry. The HV signal is applied to the inner electrode which is covered by a dielectric while the outer electrode is grounded. The gas enters through the upper slit, circulates around the inner electrode and exits through the bottom slit forming a rectangular afterglow curtain. In this configuration, only the neutral excited species created in the discharge are transported outside the reactor to reach the substrate. The vapour of the precursor (obtained by using a bubbler) is introduced in the afterglow, between the exit of the reactor and the substrate.

The direct DBD reactor is manufactured by the IST-Fraunhofer of Braunschweig (Germany). It is made of two flat parallel high voltage electrodes covered with dielectric and the substrate is placed on a grounded metallic moving table. The process gas (mixed with the vapour of the precursor) flows between the two electrodes and in the gap between the electrodes and the substrate. The reactor is also supplied by a sinusoidal high voltage generator, operating at 10 or 22.5 kHz frequency. An external trigger allows chopping the HV signal to generate ON and OFF phases.

The precursors used in the study to obtain coatings with different chemical compositions are hexamethyldisiloxane (HMDSO), decamethylpentasiloxane (DMPSO or D5), vinyltrimethoxysilane (VTMS) and maleic anhydride (MA) and are shown in Fig. 3. The reactor and the deposition conditions used for the three organo silicon coatings prepared are summarized in Table 1.

Surface Analysis Methods

Scanning electron microscopy (SEM) images were recorded using a Hitachi SU-70 field emission SEM (FE-SEM) after a 5 nm platinum deposit to avoid charging and

distortion. Fourier transform infrared Spectroscopy (FTIR) were performed with a Bruker Hyperion 2000 spectrometer equipped with a Ge-ATR-crystal accessory. X-ray photoelectron spectroscopy (XPS) analyses were realized with a Kratos Axis-Ultra instrument using a monochromatic Al Kα X-ray source (hν = 1486.6 eV) at pass energy of 20 eV for high resolution spectra. The crystalline phase composition of TiO_2 samples was determined by X-Ray diffraction (XRD) measurements carried out with a Bruker D8 instrument in a Bragg–Brentano configuration using CuK_α radiation (40 kV-40 mA).

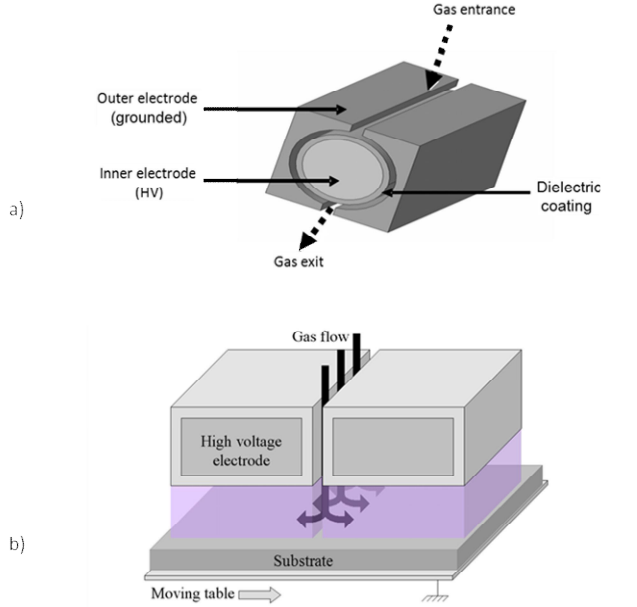

Fig. 2. Schematic of (a) remote-DBD and (b) direct plane-to-plane DBD reactors used for the synthesis of organo silicon coatings.

RESULTS AND DISCUSSION

Chromium/Iron (Cr_xFe_y) Oxides

The properties of stainless steel are based on the passive layer on the surface, which mainly consists of chromium oxides and has a thickness of about ten molecular layers (Pießlinger-Schweiger, 2005). Therefore, in our earlier molecular modelling study, the chromium-rich oxide layer of stainless steel was described by the hexagonal Cr_2O_3, the optimized lattice parameters of which are a = b = 513.8 pm, c = 1403.6 pm and c/a = 2.732 (Puhakka et al., 2008). In this study, it was considered the effect of the iron content on the surface structure of the corrosion protective Cr-rich oxide layer. It was investigated the crystal and surface structures of different Cr_xFe_y oxides, and it was supposed that Cr and Fe exist in the same phase. In Table 2, lattice parameters for hexagonal Cr_2O_3 and Fe_2O_3, and three tetragonal $Cr_8Fe_4O_{18}$ structures are shown. In the $Cr_8Fe_4O_{18}$ oxides, the substitution of Fe atoms was made for different lattice points (Fig. 4).

Earlier (Puhakka *et al.*, 2008), the fully oxided (004) surface of Cr_2O_3 was supposed to describe the surface structure of stainless steel. However, XPS analyses of stainless steel surface highlighted the presence of metallic chromium, Cr_2O_3 and $Cr(OH)_3$. This is consistent with literature data (Diawara, 2012), that the uppermost layer of stainless steel consists of Cr-$(OH)_3$ groups. Therefore, the (006) surface with three-coordinated Cr atoms was selected for our studies. On this surface, the vacant sites of Cr atom were occupied with hydroxide groups, and the surface structure was optimized in order to obtain energetically stable structures for deposition formation studies (Fig. 5).

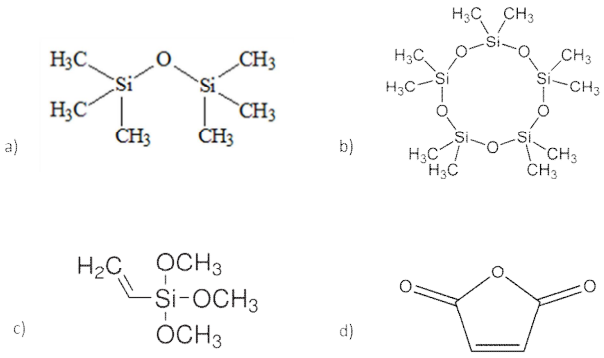

Fig. 3. Chemical formula of the precursors used for the synthesis of organo silicon coatings: (a) HMDSO, (b) D5, (c) VTMS and (d) MA.

Table 1. Deposition conditions for organo silicon coatings.

Sample Name	Reactor	Precursor	Gas process conditions	Electrical process conditions
SiOC-1	Remote DBD	D5	Gas: Nitrogen Process gas flow rate = 80 slm Carrier gas flow rate = 30 slm	130 kHz sinusoidal HV P=500 W
SiOC-2	Direct DBD	HMDSO	Gas: Nitrogen Process gas flow rate = 19,5 slm Carrier gas flow rate = 0,5 slm	22,5 kHz sinusoidal HV P=100 W
SiOC-3	Direct DBD	MA+VTMS	Gas: Argon Process gas flow rate = 4,95 slm Carrier gas flow rate (MA) = 14,8 slm Carrier gas flow rate (VTMS) = 0,25 slm	10 kHz chopped sinusoidal HV Time ON = 10 ms Time OFF = 40 ms P = 100 W

Table 2. Lattice parameters of different Cr_xFe_y oxides.

Coating	Exptl. values (pm)		Calculated values (pm)	
	a = b	c	a = b	c
Fe_2O_3	503.5	1 372.0	n/a	n/a
Cr_2O_3	495.9	1 359.3	513.8	1 403.6
$Cr_8Fe_4O_{18}$(I)			503.3	1 373.1
$Cr_8Fe_4O_{18}$(II)			504.8	1 370.4
$Cr_8Fe_4O_{18}$(III)			513.4	1 392.4

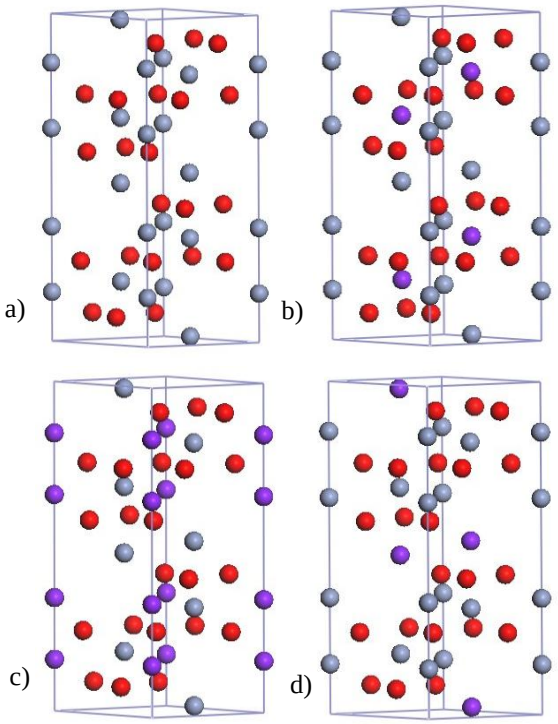

Fig. 4. The unit cells of Cr_xFe_y oxides: a) Cr_2O_3, b) $Cr_8Fe_4O_{18}$ (I), c) $Cr_8Fe_4O_{18}$ (II) and d) $Cr_8Fe_4O_{18}$ (III). Red spheres: oxygen. Grayish blue spheres: chromium. Blue spheres: iron.

Titanium Oxide Thin Films

TiO_2 may coexist in four different crystal structures: anatase, brookite, cotunnite and rutile (Diebold, 2003). Of these, rutile and anatase are the most important ones in the TiO_2 applications. In this study, XRD was used to study the crystalline phase composition of the Ti oxide coatings. The as-prepared TiO_2 is amorphous, but annealing the sample at 300 °C is sufficient to obtain crystalline TiO_2 with anatase structure (Fig. 6). SEM pictures of TiO_2 samples before and after annealing are shown in Fig. 7. Coatings present a cauliflower-like structure, and it can be observed that the morphology is not changed after annealing at 300 °C during 1 h.

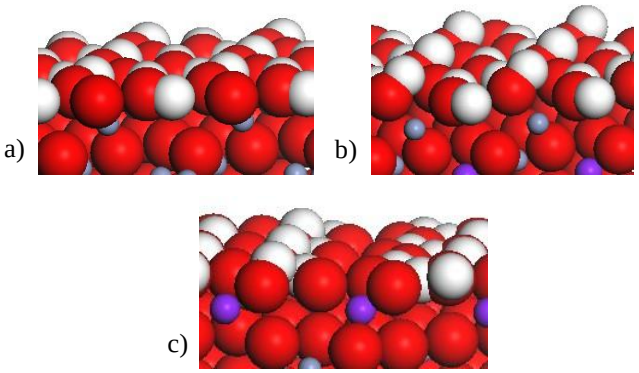

Fig. 5. a) The $Cr(OH)_3$, b) the $CrFe(OH)_3$ (I) and c) the $CrFe(OH)_3$ (III) surfaces. Red spheres: oxygen. Greyish blue spheres: chromium. Blue spheres: iron. White spheres: hydrogen.

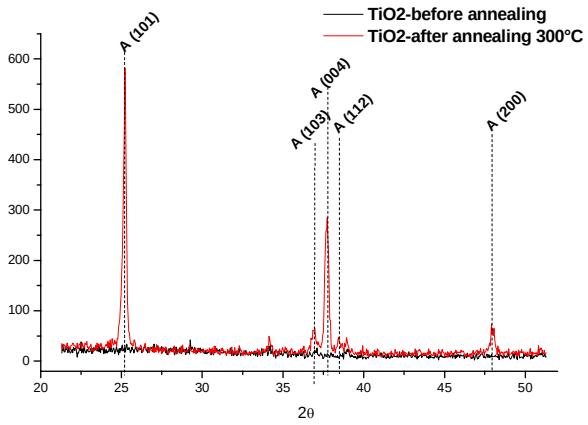

Fig. 6. XRD patterns of the deposited TiO_2 films.

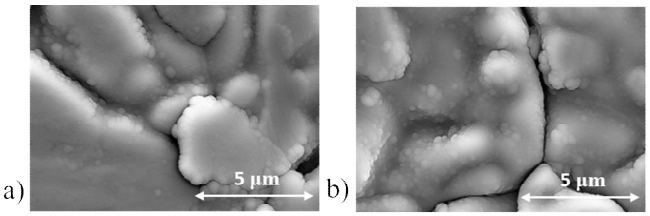

Fig. 7. Scanning electron micrographs of TiO_2 thin films (a) before and (b) after annealing.

Based on the characterization results, the focus of molecular modelling work was on the anatase surfaces, and the results of the anatase were compared to those of the rutile. The optimized lattice parameters of the tetragonal anatase are a = b = 385.4 pm and c = 1 000.0 pm. The corresponding optimized parameters for the rutile are a = b = 470.2 pm and c = 301.7 pm (Puhakka *et al.*, 2007). Of anatase surfaces, the (101) surface with four-coordinated Ti atoms, and (004) and (200) surface with five-coordinated Ti atoms were selected for deposition formation studies. Of rutile surfaces, calculations were done for the (101) surface (Fig. 8).

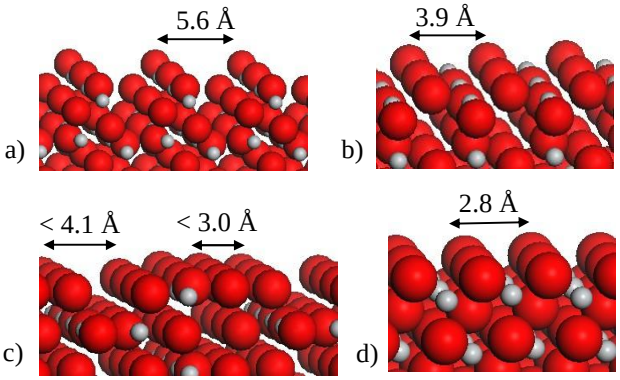

Fig. 8. TiO_2 surfaces: a) the anatase (101), b) the anatase (004), c) the anatase (200), and d) the rutile (101). Red spheres: oxygen. Grey spheres: titanium.

Organo Silicon Thin Films

In order to study organo silicon thin films by molecular modelling techniques, model surface structures have to be generated. As a starting point, our earlier optimized crystal structure of SiO_2, (a = b = c = 692.4 pm), was utilized (Puhakka et al., 2011). Based on the estimated morphology of SiO_2, the (111) surface is dominant. In addition to the basic structure of SiO_2, CH_3- and COOH-modified SiO_2 surfaces were also considered.

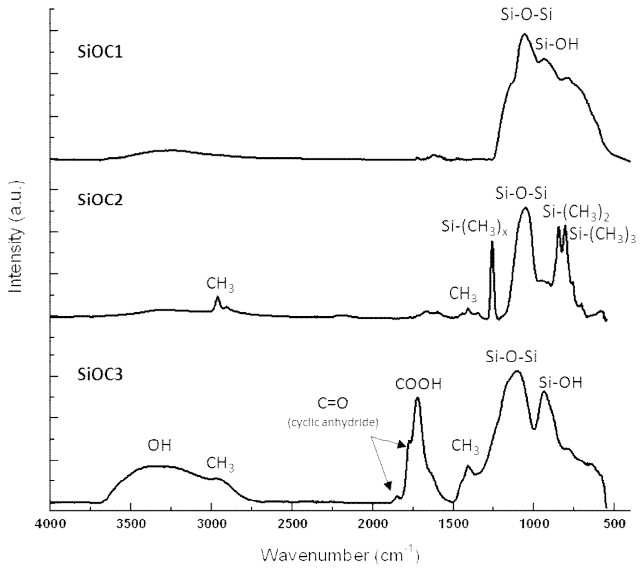

Fig. 9. Attentuated total reflectance - fourier transform infrared spectroscopy (ATR-FTIR) spectra for organo silicon coatings.

In the experimental part, the chemical composition of the deposited SiOC coatings was investigated by FTIR. The spectra obtained (Fig. 9.) reveal for all the samples the presence of a broad and intense band between 1000 and 1200 cm^{-1} which can be assigned to Si-O-Si chain vibrations. This observation confirms that polymerization occurred during the PECVD process to lead to Si-O-Si chain-based layers. However, the comparison of the three spectra highlights strong differences in the chemical structure of the films. The sample SiOC1, prepared from D5 in remote-DBD reactor presents an inorganic character with a probable SiO_2-like structure, with a part of the silicon atoms linked to hydroxyl groups. The XPS analyses (results not shown) confirmed the inorganic character of the coatings since the amount of carbon in the layer does not exceed 5%. In revenge, the atomic percentages of carbon is much more important in samples SiOC2 (~25% at.) and SiOC3 (~50% at.). In SiOC2 sample, absorptions relative to $Si(CH_3)_x$ and CH_3 vibrations are detected. It can thus be concluded that this layer presents a polydimethylsiloxane (PDMS) structure, i.e. Si-O backbone with CH_3 pendant groups as confirmed by deconvolution of the Si 2p XPS high resolution spectra well described in Boscher *et al* (2013). In the SiOC3 coating, the Si-O-Si chain is functionalized with COOH groups as clearly shown by the strong absorption peak at 1720 cm^{-1}. These COOH groups result from hydrolysis of anhydride units retained in the coating (Manakhov *et al*, 2012).

Various morphologies of the SiOC coatings can be distinguished on SEM images of Fig. 10. SiOC3 is observed to be relatively smooth and particle free whereas SiOC2 is composed of agglomerated particles with sizes varying from 200 nm to 300 nm. The layer SiOC1 presents an intermediate morphology, with a quite smooth layer with embedded small particles.

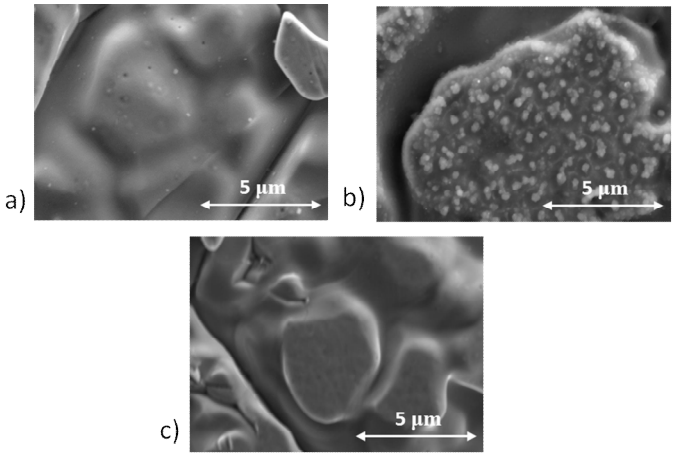

Fig. 10. Scanning electron micrographs of organo silicon thin films: (a) SiOC1 (b) SiOC2, and (c) SiOC3.

Deposition Formation on the Surfaces

In the $CaCO_3$ deposition formation studies, the initiation of crystallization fouling caused by Ca^{2+} and CO_3^{2-} species, and water as a process liquor was investigated. It was supposed that water adsorbs firstly onto surfaces, and thereafter the other species. The adsorption mechanism of water depends on the surface structure and chemical composition of surfaces. Water can adsorb onto solid surfaces as a molecule, or it can dissociate forming partially or fully hydroxylated surfaces (Cappus *et al.*, 1993; Maurice *et al.*, 2001; Henderson *et al.*, 2000; Henderson, 2002; Saunders *et al.*, 2008; Ignatchenko *et al.*, 2006).

In the case of $Cr_xFe_y(OH)_3$ surfaces, the adsorption of water was not considered, because it was supposed that the

hydroxyl group layer already describes the effect of moisture. However, in the case of Ti and Si oxides, the water adsorption was taken into account in order to stabilize surfaces before the adsorption of Ca^{2+} and CO_3^{2-} species. On the anatase (200) surface, water does not dissociate, but on the anatase (101) and (004) surfaces, water dissociates forming a hydroxylated surface structure (* represents surface oxygen atom):

$$S + H_2O \rightarrow S\text{-}O^*\text{-}H + S\text{-}OH \quad (1)$$

On the rutile (101) and SiO_2 (111) surfaces, water dissociates only partially. On the SiO_2 surface, also surface hydride groups exist in addition to surface hydroxyl groups:

$$2\ S\text{-}H_2O \rightarrow S\text{-}H_2O + S\text{-}OH + S\text{-}H \quad (2)$$

In the case of the CH_3- and COOH-modified surfaces, water does not dissociate.

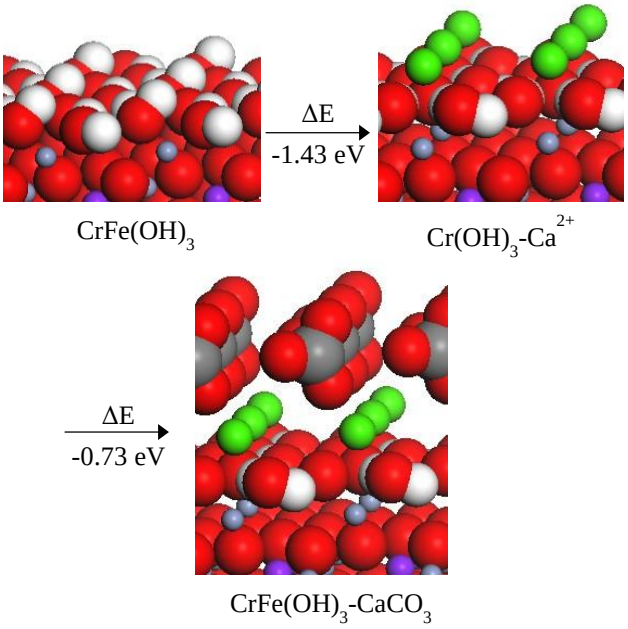

Fig. 11. Formation of $CaCO_3$ deposition on the $CrFe(OH)_3$ (I) surface. Red spheres: oxygen. Greyish blue spheres: chromium. Blue spheres: iron. White spheres: hydrogen. Green spheres: calcium. Grey spheres: carbon.

After the model surface structures were generated, primary deposition formation studies were done. The study was performed by determining the adsorption positions and energies of a Ca^{2+} ion on the surfaces, and after that a CO_3^{2-} ion was adsorbed onto the Ca^{2+} covered surfaces. By optimizing the positions of Ca^{2+} and CO_3^{2-} on the surfaces at the same time, the bonding geometry of $CaCO_3$ on the surface was achieved. As a result, the detailed reaction mechanisms were obtained for the formation of $CaCO_3$ deposition.

In Fig. 11, the formation mechanism of $CaCO_3$ deposition is presented on the $CrFe(OH)_3$ (I) surface, and in Fig. 12 on the anatase (200) surface. In Fig. 13, $CaCO_3$ depositions on different SiO_2 surfaces are shown. The energetics of all the investigated surface materials are presented in Table 3. Energetics for the growth of calcite ($CaCO_3$) surface is also included into the results.

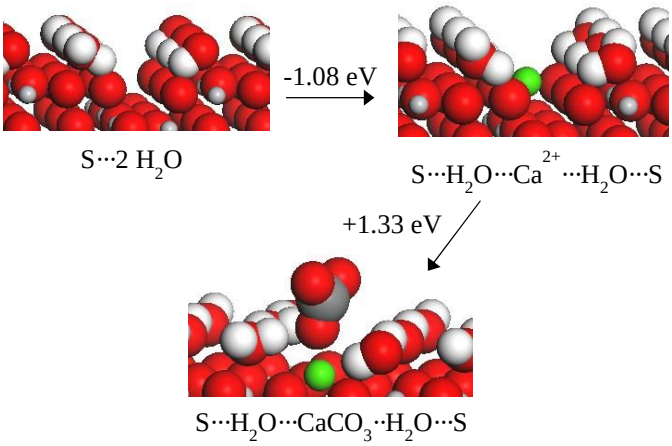

Fig. 12. Formation of $CaCO_3$ deposition on the anatase (200) surface. Red spheres: oxygen. Small grey spheres: titanium. White spheres: hydrogen. Green spheres: calcium. Big grey spheres: carbon.

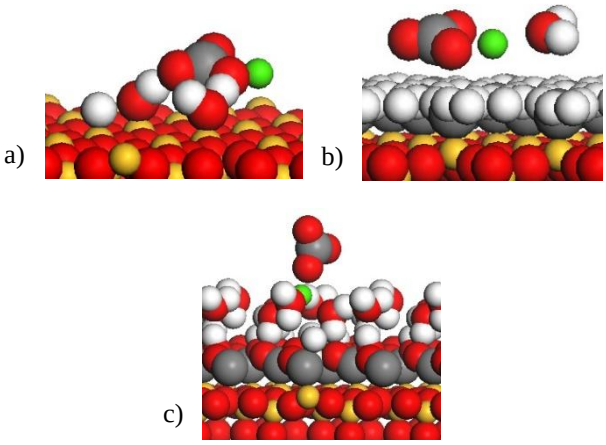

Fig. 13. $CaCO_3$ deposition on SiO_2 (111) surfaces: a) ideal, b) CH_3-modified, and c) COOH-modified. Red spheres: oxygen. Yellow spheres: silicon. White spheres: hydrogen. Green spheres: calcium. Grey spheres: carbon.

Molecular modelling results were compared to results received from fouling experiments (Riihimäki, 2013). In the experiments, induction time (t_{ind}) of fouling for deposited coatings were defined using a laboratory set-up described by Riihimäki *et al.*, 2010. Test solution was prepared by mixing equivalent amounts (0.5 g/dm^3) of $CaCl_2{\cdot}2H_2O$ and $NaHCO_3$ salts with deionized water and mixing them together. Titanium thin films were tested with 72 kWh heat flux, and organo silicon thin films with 80 kWh heat flux.

On the anatase type surface after annealing, t_{ind} = 140 min was observed. This reveals that anatase allows to delay the beginning of $CaCO_3$ deposit on surface in comparison with the uncoated stainless steel (t_{ind} = 90 min). This is in accordance with the molecular modelling results which indicate that deposition formation energies of $CaCO_3$ are higher on the anatase surfaces than on the $Cr(OH)_3$, Cr_2O_3

and $CrFe(OH)_3$ surfaces. The next step in coating deposition will consist in the synthesis of textured TiO_2 surfaces with preferential orientations. Experimental fouling results obtained with these textured surfaces could strengthen the molecular modelling calculations presented in this study.

Besides, fouling tests revealed that amorphous TiO_2 seems also to be very promising since t_{ind} = 200 min was measured. For now, we do not have explanations for this observation. More surface characterization and calculations are needed to go further in the comprehension of this observed phenomenon.

Table 3. Deposition formation energies for CaCO3.

	ΔE (eV)	Bonding type
SiO_2 (111) with COOH	0.93	$S^{\cdots}(H_2O)_3^{\cdots}Ca^{2+}$
Anatase (200)	0.25	$S–Ca^{2+}$
Anatase (101)	0.14	$S–OH^{\cdots}Ca^{2+}$
$Cr(OH)_3$ with CO_2	0.25	$S^{\cdots}(CO_2)_3^{\cdots}Ca^{2+}$
SiO_2 (111) with CH_3	-0.57	$S–Ca^{2+}$
Anatase (004)	-0.68	$S–Ca^{2+}$
$Cr(OH)_3$	-1.03	$S–Ca^{2+}$
$CaCO_3$	-2.13	$S–Ca^{2+}$
$CrFe(OH)_3$ *(Cr above Fe)*	-2.16	$S–Ca^{2+}$
Rutile (101)	-2.25	$S–OH^{\cdots}CaCO_3^{\cdots}HO–S$
Cr_2O_3 with water	-3.15	$S^{\cdots}(H_2O)_3^{\cdots}Ca^{2+}$
$CrFe(OH)_3$ *(Fe above Cr)*	-4.04	$S–Ca^{2+}$
SiO_2	-7.98	$S–OH^{\cdots}CO_3$

For the conditions used in the fouling experiments for SiOC coatings, t_{ind} on uncoated stainless steel was equal to 135 min. The sample SiOC1 (SiO_2-like structure) revealed very poor fouling resistance since formation of $CaCO_3$ deposition started at the really beginning of the experiment (t_{ind} = 0 min). An increase of fouling resistance was observed for the layer SiOC2 (Si-O-Si backbone with CH_3 pendant groups) with t_{ind} = 80 min, but the best behaviour was obtained for SiOC3 coating (Si-O-Si backbone with COOH functionalization). During the 1 200 min test period, no $CaCO_3$ deposition occurred on the surface. This means that t_{ind} is at least around 10 times higher than for uncoated stainless steel. This kind of deposit on the surface is really promising to mitigate fouling.

These experimental observations are quite well fitting with molecular modelling results indicating deposition formation energies of -7.98 eV, -0.57 eV and 0.93 eV for SiO_2, SiO_2 with CH_3 and SiO_2 with COOH, respectively. However, it is important to keep in mind that the structure of the deposited layer is not crystallized as in the calculations. Moreover, the surface morphologies of the layers are different for the three deposits, and it may play an important role. For this reason, samples with various morphologies (smooth, rough, granular-shaped) but with the same chemical compositions are being developed for forthcoming studies to evaluate the influence of this property on fouling.

CONCLUSIONS

Development of the coatings was focused on laboratory tailored TiO_2 (PVD) and SiOC based (AP-PECVD) coatings. Surface characterization of coatings, molecular modelling of deposition formation and fouling experiments for deposited samples indicated that TiO_2 (anatase and amorphous) and COOH-functionalized SiOC coatings seem to be promising materials for mitigation of fouling caused by $CaCO_3$. Additional development of coatings are still needed in order to clarify the effect of textured surface structures, various morphologies and trace compounds on the $CaCO_3$ deposition formation.

ACKNOWLEDGEMENTS

The authors wish to acknowledge Mr Markus Riihimäki from University of Oulu for fouling experiments. The communication with Dr David Duday and Dr Jérôme Guillot from CRP-Gabriel Lippmann are gratefully acknowledged. This study was financially supported in the MATERA+ ERA-Net co-operation by the Functional materials programme of Tekes, the INTER programme of FNR, and industrial partners e.g. Andritz, Oerlikon Balzers and Outokumpu.

NOMENCLATURE

AP-PECVD	Atmospheric Pressure - Plasma Enhanced Chemical Vapour Deposition
ATR-FTIR	Attentuated Total Reflectance - Fourier Transform Infrared Spectroscopy
CASTEP	CAmbridge Serial Total Energy Package
DBD	Dielectric Barrier Discharge
dcMS	direct current Magnetron Sputtering
DMPSO/D5	Decamethylpentasiloxane
FE-SEM	Field Emission - Scanning Electron Microscopy
FTIR	Fourier Transform Infrared Spectroscopy
GGA-PBE	Perdew, Burke and Ernzerhof version of generalized gradient approximation functional
GGA-RPBE	Hammer, Hansen, Norskov modified Perdew, Burke and Ernzerhof version of generalized gradient approximation
HMDSO	Hexamethyldisiloxane
HV	High-Voltage
MA	Maleic Anhydride
PDMS	Polydimethylsiloxane
PECVD	Plasma Enhanced Chemical Vapour Deposition
PVD	Physical Vapour Deposition
SEM	Scanning Electron Microscopy
t_{ind}	Induction Time
VTMS	Vinyltrimethoxysilane
XPS	X-ray Photoelectron Spectroscopy
XRD	X-Ray Diffraction

REFERENCES

Accelrys, 2009, *MS Modeling*, Release 5.0. San Diego: Accelrys Software Inc.

Accelrys, 2011, *MS Modeling*, Release 6.0. San Diego: Accelrys Software Inc.

Boscher, N. D., Duday, D., Verdier, S., and Choquet, P., 2013, Single-step process for the deposition of high water contact angle and high water sliding angle surfaces by atmospheric pressure dielectric barrier discharge, *ACS Appl. Mater. Interfaces*, Vol 5, pp. 1053-1060.

Bott, T. R., 1995, *Fouling of Heat Exchangers*, Elsevier, Amsterdam.

Cappus, D., Ehrlich, C. X. D., Dillmann, B., Ventrice, C. A. Jr., Shamery, K. A., Kuhlenbeck, H., and Freund, H.-J., 1993, Hydroxyl groups on oxide surfaces: NiO(100), NiO(111) and Cr_2O_3(111), *Chem. Phys.*, Vol. 177, pp. 533–546.

Diawara, B., 2012, Multiscale modeling of the growth of passive layer on stainless steels: Kinetic Monte Carlo simulation based on quantum mechanics and force field data, *Abstract Volume*, International Conference on Multiscale Approaches for Process Innovation – MAPI, IFP Energies nouvelles-Lyon, France, 25–27 January, 2012.

Diebold, U., 2003, The surface science of titanium dioxide, *Surf. Sci. Rep.*, Vol. 48, pp. 53–229.

Henderson, M. A., and Chambers, S. A., 2000, HREELS, TPD and XPS study of the interaction of water with the α-Cr_2O_3(001) surface, *Surf. Sci.*, Vol. 449, pp. 135–150.

Henderson, M. A., 2002, The interaction of water with solid surfaces: fundamental aspects revisited, *Surf. Sci. Rep.*, Vol. 46, pp. 1–308.

Ignatchenko, A., Nealon, D. G., Dushane, R., and Humphries, K., 2006, Interaction of water with titania and zirconia surfaces, *J. Mol. Cat. A: Chem.*, Vol. 256, pp. 57–74.

Kostoglou, M., and Karabelas, A. J., 1998, Comprehensive Modeling of Precipitation and Fouling in Turbulent Pipe Flow, *Ind. Eng. Chem. Res.*, Vol. 37, pp. 1536–1550.

Leach, A. R., 2001, *Molecular Modelling, Principles and Applications*, 2nd ed., Pearson Education Limited, Essex.

Manakhov, A., Moreno-Couranjou, M., Boscher, N. D., Rogé, V., Choquet, P., and Pireaux, J-.J., 2012, Atmospheric pressure pulsed plasma copolymerization of maleic anhydride and vinyltrimethoxysilane: Influence of electrical parameters on chemistry, morphology and deposition rate of the coatings, *Plasma Processes and Polymers*, Vol 9, pp. 435–445.

Maurice, V., Cadot, S., and Marcus, P., 2001, Hydroxylation of ultra-thin films of α-Cr_2O_3 (0 0 0 1) formed on Cr (1 1 0), *Surf. Sci.*, Vol. 471, pp. 43–58.

Müller-Steinhagen, H., 2002, *Heat Exchanger Fouling – Fundamental Approaches and Technical Solutions*, Publico Publications, Essen. p, XI.

Mwaba, M. G., Golriz, M. R., and Gu, J., 2006, A semi-empirical correlation for crystallization fouling on heat exchange surfaces, *App. Therm. Eng.*, Vol. 26, pp. 440–447.

Pießlinger-Schweiger, S., 2005, Surface treatment of metallic heat exchangers, *Heat Exchanger Fouling and Cleaning - Challenges and Opportunities*, Kloster Irsee, Germany, June 5 – 10, 2005, Engineering Conferences International, Brooklyn, NY, USA.

Puhakka, E., Riihimäki, M., and Keiski, R. L., 2007, Molecular Modeling Approach on Fouling of the Plate Heat Exchanger: Titanium Hydroxyls, Silanols, and Sulphates on TiO_2 Surfaces, *Heat Transfer Eng.*, Vol. 28, pp. 248–254.

Puhakka, E., Riihimäki, M., and Keiski, R. L., 2008, Fouling mechanisms by *ab initio* calculations – Condensation reactions on the rutile (101) surface and adsorption of ions on the Cr_2O_3 surfaces, *Proceedings of the 7th International Conference on Heat Exchanger Fouling and Cleaning – Challenges and Opportunities*, eds. H. Müller-Steinhagen, M. R. Malayeri, and A. P. Watkinson, ECI Symposium series, Tomar, Portugal, July 1–6, 2007, The Berkeley Electronic Press, Vol. RP5, pp. 300–307.

Puhakka, E., Riihimäki, M., Pääkkönen, T., and Keiski, R. L., 2011, Density Functional Theory Studies on the Formation of $CaCO_3$ Depositions on Cristobalite, Diamond, and Titanium Carbide surfaces, *Heat Transfer Eng.*, Vol. 32, pp. 282–290.

Puhakka, E., Riihimäki, M., Keiski, R.L., 2012, The effect of magnesium on the formation of $CaCO_3$ depositions, *Proceedings of International Conference on Heat Exchanger Fouling and Cleaning – 2011 (Peer-reviewed)*, eds. M. R. Malayeri, H. Müller-Steinhagen, and A. P. Watkinson, Crete Island, Greese, June 05–10, 2011, EUROTHERM, pp. 243–250.

Pääkkönen, T. M., Riihimäki, M., Puhakka, E., Muurinen, E., Simonson, C. J., and Keiski, R. L., 2010, Crystallization fouling of $CaCO_3$ – Effect of bulk precipitation on mass deposition on the heat transfer surface, *Proceedings of 8th International Conference on Heat Exchanger Fouling and Cleaning – 2009 (Peer-reviewed)*, eds. H. Müller-Steinhagen, M. R. Malayeri, and A. P. Watkinson, EUROTHERM Seminar No. 86 on Heat Exchanger Fouling and Cleaning – 2009, Schladming, Austria, June 14–19, 2009, EUROTHERM, pp. 209–216.

Riihimäki, M., 2013, Personal communications.

Riihimäki, M., Ojaniemi, U., Pättikangas, T. J. H., Pääkkönen, T. M., Manninen, M., Puhakka, E., Muurinen, E., Simonson, C. J., and Keiski, R. L., 2010, Fouling in high solid content suspension – Effect of nucleating air and background electrolyte, *Proceedings of 8th International Conference on Heat Exchanger Fouling and Cleaning VIII – 2009 (Peer-reviewed)*, eds. H. Müller-Steinhagen, M. R. Malayeri, and A. P. Watkinson, EUROTHERM Seminar No. 86, Schladming, Austria, June 14–19, 2009, pp. 192–199.

Saunders, S. R. J., Monteiro, M., and Rizzo, F., 2008, The oxidation behaviour of metals and alloys at high temperatures in atmospheres containing water vapour: A review, *Prog. Mater. Sci.*, Vol. 53, pp. 775–837.